

# Development of an experimental facility for the study of microparticle initiated radio-frequency vacuum breakdown

R. Casagrande,<sup>1,2,3,a)</sup> H. Faugel,<sup>2</sup> F. Fischer,<sup>2</sup> H. Fünfgelder,<sup>2</sup> F. Riedl,<sup>2</sup> G. Siegl,<sup>2</sup> P. Bettini,<sup>3</sup> J.-M. Noterdaeme,<sup>1,2</sup> and K. Crombé<sup>1,4</sup>

<sup>1)</sup>*Department of Applied Physics, Ghent University, 9000 Gent, Belgium*

<sup>2)</sup>*Max-Planck-Institut für Plasmaphysik, 85748 Garching, Germany*

<sup>3)</sup>*Università degli Studi di Padova, 35122 Padova, Italy*

<sup>4)</sup>*Laboratory for Plasma Physics, ERM/KMS, 1000 Brussels, Belgium*

(Dated: 8 December 2020)

An ongoing objective in ion cyclotron range of frequencies (ICRF) systems is the improvement of power coupling to the plasma. During the last decade, this goal has been mainly pursued through the study of the coupling resistance, either by optimizing the antenna layout or by tailoring the Scrape-Off Layer (SOL) profile with gas puffing. Another approach is to increase the voltage handling capability of the ICRF system, limited by breakdown in the launchers or in the transmission lines. This paper describes the design of IBEX, a device to investigate fundamental aspects of radio-frequency arcs in ICRF-relevant conditions. IBEX can achieve a peak voltage of 48 kV at 54 MHz, with 5 kW input power.

## I. INTRODUCTION

In next generation fusion devices, in order to meet the tritium breeding ratio requirements, heating systems with reduced impact on the breeder volume will be required<sup>1</sup>. If the port-plug antenna design adopted for ITER is maintained for future reactors, the requirement of a small footprint will inevitably lead to high power density launchers, and in turn to high voltages on the ICRF system. The ITER antenna, coupling 20 MW to the plasma in the 40–55 MHz frequency range, will have a maximum voltage on the straps<sup>2</sup> in excess of 40 kV. In case of an in-port solution for DEMO, electric field limits will also be major design issues. It is then desirable to extend the range of operational voltage and electric field in ICRF systems, not only to reduce design complexity but also to improve the reliability of antennas.

A device dedicated to the study of fundamental mechanisms of radio-frequency arcs has been developed at the Max-Planck-Institut für Plasmaphysik in Garching - Germany, with the aim of gaining improved information on voltage limits of ICRF launchers. In this paper we describe the design of ICRF Breakdown EXperiment (IBEX), particularly focusing on the development of an RF system able to meet the voltage and frequency requirements.

## II. ICRF ENVIRONMENT

### A. Operational limits

The voltage limit imposed by ITER Organization (IO) on the ICRF system is 45 kV, with a maximum electric field of 2 kV/mm along the magnetic field lines and 3

kV/mm on all the other locations<sup>2</sup>. These boundaries are extrapolated from the operational conditions of existing antennas, hence the strategy to ensure reliability and availability is to provide a reasonably large margin on the main macroscopic parameters affecting the breakdown in known systems. However, arcs in ICRF antennas are still poorly understood, due to the complexity and the range of spurious interactions the tokamak environment can give rise to, and the difficulty of direct observation and diagnosis of breakdown inside the antenna box. Significantly higher electric fields, with respect to the ones established by IO, are routinely achieved in closed vacuum environments, e.g. RF cavities for particle accelerators, where extremely good control over the surface conditions can be obtained. Conversely, ICRF launchers can be subjected to dust contamination due to erosion of plasma-facing components, as well as plasma interaction during intense transient events such as Edge Localized Modes (ELMs)<sup>3</sup>. Studies on the effect of plasma interaction on voltage stand-off have been carried out in ASDEX Upgrade with an RF probe<sup>4</sup>, providing some insights on the observed correlation between ELMs and antenna breakdown. On the other hand, the effect of microparticles on the voltage holding of ICRF launchers has not been explored in detail yet, both concerning particulate contamination and dust impact on the antenna.

### B. Dust deleterious effects

Microparticles are well known to affect the voltage holding of vacuum insulated gaps, either by producing enhanced field emission sites if deposited on the electrodes surface, or by being accelerated by the background electric field, which in turn can lead to evaporation of the particle or formation of craters upon impact with the electrodes<sup>5</sup>. The latter is usually not a relevant phenomenon in RF structures, since the charge to mass ratio of typically encountered particles does not allow for

---

<sup>a)</sup>Electronic mail: riccardo.casagrande@ipp.mpg.de

enough acceleration during half RF period. Nonetheless, large amounts of particulate is generated in nuclear fusion reactors<sup>6–8</sup>, which can reach the ICRF launchers. Microparticles can be remobilized and deposited on the antenna surface, or be subjected to acceleration in the edge plasma, reaching velocities up to several hundred of m/s prior to the vaporization or impact with the plasma-facing components<sup>9</sup>. IBEX aims at providing a test platform to investigate the parameters that can influence voltage holding, specifically in ICRF relevant conditions, focusing on microparticle contamination during the initial experimental phase.

### III. EXPERIMENT SPECIFICATIONS

#### A. Main requirements

The main requirement of IBEX is to provide voltage and electric field conditions at the test electrodes at and above the typical limits of ICRF systems. Since these values can greatly vary between different machines, the limitations on ITER ICRF were considered as design basis. Other requirements include background pressure well below the typical observed limits for modified multipactor discharge, i.e. less than  $10^{-4}$  mbar<sup>10</sup>. IBEX should also guarantee a quick replacement of the test electrodes and have the possibility to interface with a microparticle injection system.

#### B. Experiment outline

High voltages in the frequency range of interest can be obtained by generating a standing wave pattern in a coaxial transmission line. The maximum voltage standing wave ratio (VSWR) is achieved in resonant conditions: in IBEX, a  $\lambda/4$  coaxial resonator is used to obtain a high RF voltage on the test electrodes, positioned at the open-end. The terminal part of the resonator is composed of a vacuum piping section and connected to a pumping system, to achieve experimental pressures below  $10^{-4}$  mbar. Vacuum tightness and electrical continuity are ensured by a coaxial ceramic feedthrough in the initial segment of the transmission line. A linear manipulator allows the precise adjustment of the electrodes gap. Several access ports are available in the test chamber, to provide a direct view on the electrodes and an interface with the microparticle accelerator. The experiment is powered through a 5 kW solid-state amplifier (SSA), connected to the feeding point via:

- RF switch: allows the connection of a network analyzer to the resonator, to perform the tuning procedure.
- Directional coupler: monitoring of forward and reflected power.

- Bias-Tee: guarantees electrical separation between DC and RF circuit. This allows the DC biasing of the transmission line (e.g. for glow discharge conditioning), and measurement of the rectified field emission current, other than providing protection to the SSA.

RF voltage and current in the resonator are monitored through capacitive and inductive probes. For impedance matching, a variable vacuum capacitor is used. Figure 1 shows the basic outline of IBEX.

### IV. GENERATION OF HIGH RF VOLTAGE

#### A. Quality factor and standing wave maximum

A key aspect in the design of IBEX was the maximization of the voltage on the test electrodes, given the limited 5 kW input power ( $P_i$ ). In a quarter wavelength coaxial resonator (figure 2) with constant characteristic impedance ( $Z_0$ ), assuming a perfect matching with the source output impedance and a total reflection of the wave at the extremes, the peak voltage at the open end can be estimated as

$$V_{open} = \sqrt{\frac{8P_i Q Z_0}{\pi}}. \quad (1)$$

The maximization variables for  $V_{open}$  are then the characteristic impedance and the quality factor ( $Q$ ).  $Q$  represents the ratio between stored and dissipated energy in a RF cycle. For a coaxial transmission line with phase constant  $\beta$  and attenuation constant  $\alpha$ , the value of  $Q$  arising from resistive losses in the conductors is

$$Q_{TL} = \frac{\beta}{2\alpha} = \frac{2\pi}{\lambda R_{TL}}, \quad (2)$$

with  $R_{TL}$  resistance per unit length of the transmission line. In IBEX, the main contribution in terms of power losses per RF cycle comes from the vacuum section of the resonator, since it is composed of stainless steel piping segments with an inner diameter of 153 mm acting as the outer conductor. To minimize losses and to achieve good vacuum compatibility, the inner conductor material was chosen to be oxygen-free copper. The resistance per meter of the mixed-materials coaxial line can be expressed as

$$R_{TL} = \sqrt{\frac{f\mu_0}{\pi}} \left( \frac{\sqrt{\mu_{in}\rho_{in}}}{d_{in}} + \frac{\sqrt{\mu_{out}\rho_{out}}}{d_{out}} \right). \quad (3)$$

With  $d$ ,  $\mu$  and  $\rho$  respectively the diameter, permeability and resistivity, subscripts identifying the inner or outer conductor. The lower conductivity of the coaxial line outer conductor is not extremely penalizing in terms of power losses, due to the larger penetration depth and cross sectional area.  $Z_0=116 \Omega$  yields the optimal unloaded  $Q$ , although the maximum voltage at the resonator open end, given by eq. 1, is achieved with a

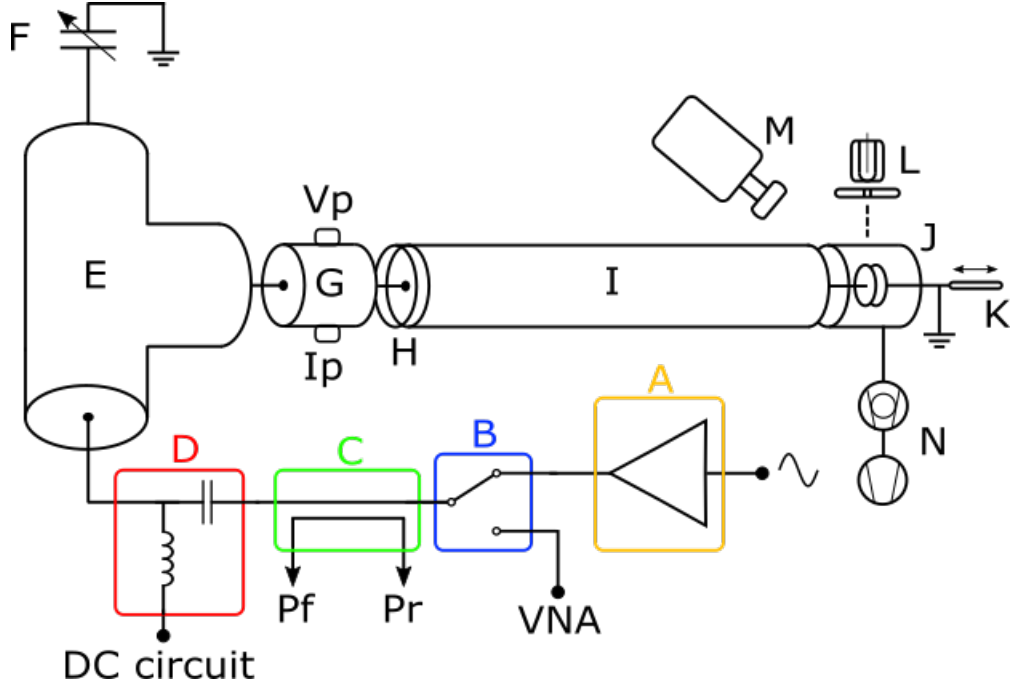


FIG. 1: IBEX schematic representation. A) Solid-state amplifier B) RF switch C) Directional coupler D) Bias tee E) 9" transmission line T section F) Tuning vacuum capacitor G) Voltage and current probes H) Vacuum feedthrough I) High impedance transmission line section J) Test electrodes K) Linear manipulator L) Microparticle source M) High speed camera N) Pumping system

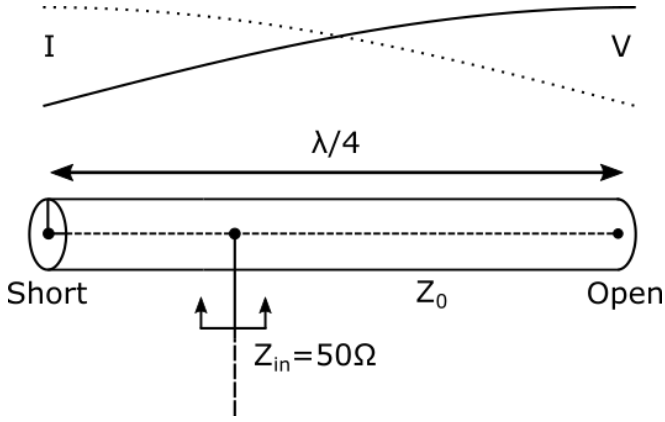


FIG. 2: Voltage and current distribution in a quarter-wavelength coaxial resonator

lower quality factor, for a characteristic impedance of  $167 \Omega$  (figure 3). Therefore, the vacuum section of the transmission line (figure 1-I) must have high characteristic impedance, hereinafter referred to as  $Z_{0,vs}$ .

## B. Matching network

For maximum power transfer, the input impedance of the resonator needs to be matched to the  $50 \Omega$  output of the amplifier ( $Z_{amp}$ ). In IBEX, this is performed with

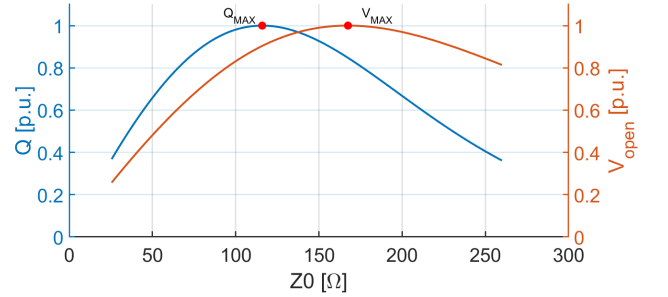


FIG. 3:  $Z_0$  dependence of Q factor and open-end voltage in a  $\lambda/4$  coaxial resonator

a variable vacuum capacitor connected in parallel to the open-ended coaxial line. The reactance seen from the feeding point can be increased by adding a section of transmission line (shorter than  $\lambda/4$ ) in series with the vacuum capacitor, thus reducing its contribution to the matching capacitance and therefore increasing  $Q$ .

Referring to the scheme in figure 4, resonance and matching are achieved for the following condition:

$$Y_{in} = \frac{1}{Z_{amp}} = Y_{vs} + Y_{mn} = Y_{vs} \tanh(\gamma_{vs} L_{vs}) + \frac{j\omega C_{tun} + Y_{mn} \tanh(\gamma_{mn} L_{mn})}{Y_{mn} + j\omega C_{tun} \tanh(\gamma_{mn} L_{mn})}. \quad (4)$$

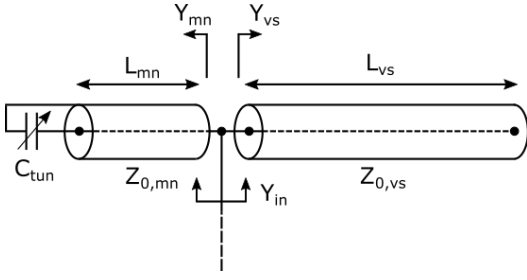


FIG. 4: Schematic representation of resonator and matching network

$L$ ,  $\gamma$ ,  $Z_0$  and  $Y$  are respectively the length of the transmission line, its propagation constant, its characteristic impedance and the admittance seen from the reference points in figure 4. Subscripts denote the matching network, vacuum section and input.

For a fixed length of the transmission lines, equation 4 has two solutions. The maximum  $Q$  in this configuration is always achieved for the higher of the two resonant frequencies. Figure 5 represents how the matching condition is reached.

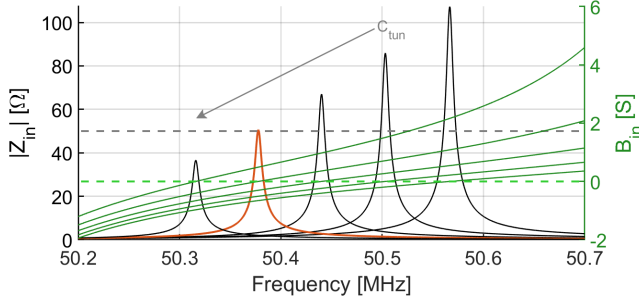


FIG. 5: Approaching the resonant and maximum power transfer conditions through variation of the tuning capacitance.  $C_{tun}$  is varied stepwise until the input susceptance ( $B_{in}$ ) is zero. Maximum power transfer is achieved when the input impedance at resonance equals  $Z_{amp}$

### C. Circuit analysis

The actual IBEX setup is more complex than the simplified schemes used for preliminary design considerations in sections IV A, IV B. The presence of a lumped tuning capacitor, changes in characteristic impedance and ceramic supports do not allow for a direct evaluation of the maximum voltage with equation 1. To study the resonator behaviour and predict the maximum achievable voltage in the realistic setup, a circuit model was developed in QucsStudio<sup>11</sup>. Given a fixed physical length of the transmission lines, the resonant frequency and the open-end voltage were investigated, depending on the

characteristic impedance of the vacuum section and the capacitance introduced by the test electrodes. Matching was achieved through minimization of S11, using the tuning capacitance as optimization variable. With respect to the optimal characteristic impedance estimated in section IV A, the maximum voltage in the realistic configuration is achieved at higher  $Z_{0,vs}$  (Figure 6). Due to mechanical constraints, a compromise had to be made between maximization of the open-end voltage and sufficient support of the inner conductor, which is cantilevered from the ceramic feedthrough. The inner conductor diameter in the vacuum section of the resonator was thus chosen to be 12 mm, leading to a characteristic impedance of 153  $\Omega$ .

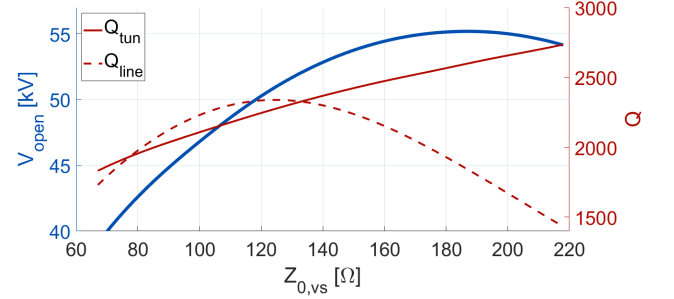


FIG. 6: Simulated voltage at the open-end of the resonator and  $Q$  factor of transmission line and tuning capacitor as a function of  $Z_{0,vs}$ , for 5 kW input power

The electrode capacitance ( $C_{el}$ ) can also significantly influence the  $Q$  factor, thus the peak voltage achievable. In particular, the resistance to ground ( $R_{gnd}$ ) plays a major role on the system performances, when considering the capacitance introduced by the test electrodes. For higher  $C_{el}$ , the leakage current to ground is increased, reducing the  $Q$  factor with a magnitude which depends on  $R_{gnd}$ . When the electrodes capacitance becomes sufficiently small,  $Q$  stabilizes to a value depending on the quality factor of the tuning capacitor and transmission line; this threshold is also conditioned by the resistance to ground (figure 7).

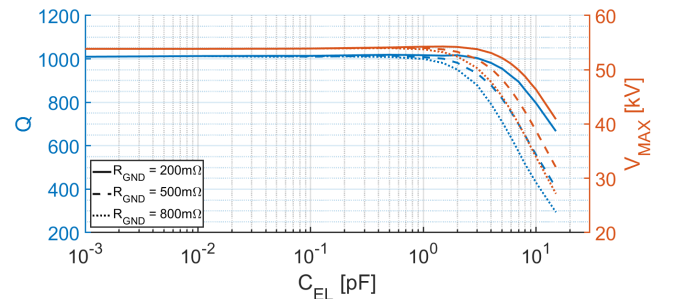


FIG. 7: Dependence of quality factor and open-end voltage on  $C_{EL}$  and  $R_{GND}$ , for  $Z_{0,vs} = 153 \Omega$

TABLE I: Parameters for microparticle injection studies

Electrode material	Stainless steel
Microparticles composition	Tungsten
Microparticles velocity	< 1000 m/s
Microparticles size	0.5 - 30 $\mu\text{m}$

## V. MICROPARTICLE SOURCE

### A. Requirements

Microscopic dust particles are produced in all magnetic confinement fusion devices, due to plasma/surface interactions. Dust dynamics can be significantly affected by the edge plasma, accelerating the particles to mean velocities exceeding 100 m/s<sup>12</sup>. Hypervelocity dust impact events have been recorded in tokamaks, even though at lower rate, indicating that microparticles can reach velocities > 1 km/s<sup>13,14</sup>. Dust analysis in several machines indicate that a dominant fraction of the particles consist of plasma-facing materials, with morphology varying from spheroids to irregular shapes<sup>7</sup>. Theoretical modelling and experimental evidence indicate that microparticles accelerated in a high voltage vacuum gap can trigger the breakdown through a variety of processes. Microparticle injection experiments, both at hypervelocity<sup>15</sup> and low velocity<sup>16</sup>, defined a range of microparticles parameters for which the trigger discharge is most likely to occur. Considering the typical dust size and velocity observed in tokamaks, experimental findings regarding microparticle triggered discharges and ICRF antennas materials, the set of parameters in table I have been defined for particle injection studies in IBEX.

### B. Design of the dust source

For particle acceleration up to the velocity range defined in table I, an electrostatic source<sup>17</sup> was developed. A reservoir containing the microparticles and a microtip are kept at high potential. A beam triode allows to switch the reservoir potential to ground. During this phase the dust is lifted inside the chamber, with a fraction depositing on the charging tip. Here the microparticles acquire a high charge, and upon detachment from the tip are accelerated through a pinhole aperture in the reservoir. A grounded extraction plate completes the acceleration, leading to an einzel lens for beam focusing. For a charging tip of radius  $r_T$  and a particle of radius  $r_P < r_T$ , the velocity acquired by the microparticle can be estimated<sup>18</sup> as in equation 5.

$$v_P = \frac{\pi V}{r_P + r_T} \sqrt{\frac{\epsilon_0 r_T}{\rho r_P}}. \quad (5)$$

This assuming, as in the setup above, that the accelerating and charging voltages ( $V$ ) are equal. Figure 8

shows the maximum velocities achievable by tungsten microparticles, accelerated by a 25 kV potential. The experimentally observed velocities are in general lower than the estimate given by equation 5, due to the incomplete charging of particles.

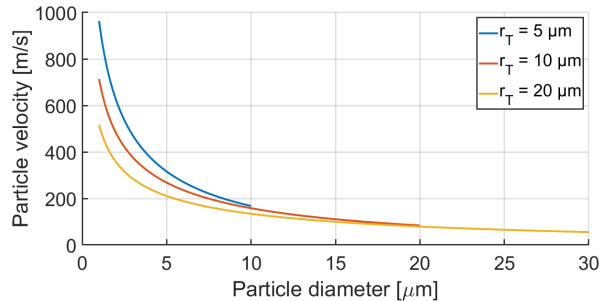


FIG. 8: Maximum velocity of microparticles for  $V = 25\text{kV}$

The charging voltage is limited by field emission and field evaporation, respectively for negative and positive charging<sup>19</sup>. Field evaporation of tungsten at room temperature occurs in the 5 MV/ $\text{\AA}$  range, whereas discharge of the microparticle due to field emission happens at one order of magnitude lower electric fields. To achieve higher charging (and accelerating) potential and to reduce the breakdown probability, microparticles are charged positively. The maximum charging voltage achievable, given the field evaporation limit of 5 MV/ $\text{\AA}$  ( $E_{ev}$ ), is

$$V_{max} = \frac{E_{ev} r_T}{k}, \quad (6)$$

in which  $k$  is an amplification factor depending on  $r_T/r_P$ . For the smallest microtip radius considered (5  $\mu\text{m}$ ) and the highest  $r_T/r_P$ , the absolute voltage limit is 100 kV. The actual constraint in terms of potential is instead defined by the pulse modulating triode, capable of handling a maximum voltage of 30 kV.

## VI. TEST ELECTRODES

### A. Electrodes for microparticle deposition experiments

Plane-parallel electrode configuration was chosen to investigate the effect of microparticle contamination on the breakdown rate. This geometry allows for simple surface preparation with standard grinding and polishing metallographic techniques. Given the performances foreseen for IBEX in terms of maximum voltage and experimentally observed RF breakdown fields in vacuum<sup>20</sup>, the gap considered is below 2.5 mm. For electrodes diameter of 40 mm and the aforementioned spacing, the field enhancement at the edges is not extremely pronounced. Therefore, a Borda profile was chosen to minimize the edge effect (figure 9) and to maintain a more compact footprint

with respect to Rogowski and Bruce profiles. A smaller size was desirable to lower the stress on the cantilevered inner conductor of the resonator and due to limitations on the sample dimensions allowed in the Scanning Electron Microscope (SEM).

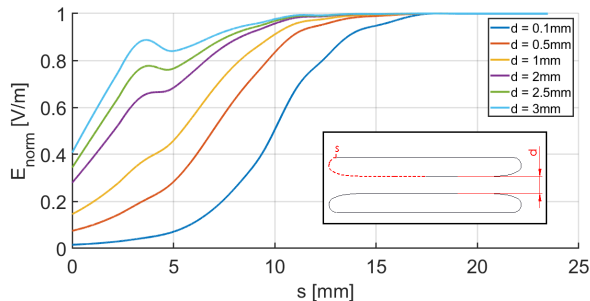


FIG. 9: Normalized surface electric field distribution for different electrodes spacing

## B. Electrodes for microparticle injection experiments

To provide an impact surface for the microparticles injected from the dust accelerator, which is installed orthogonally with respect to the axis of the resonator, a point-plane electrode configuration is used. The pointed electrode is a truncated cone terminating in a 2 mm diameter hemisphere. Figure 10 represents the two geometries chosen for experiments.

## C. Capacitance of the test electrodes

Following the considerations of section IV C, capacitance of the two electrode configurations has been computed with finite element method (figure 11).

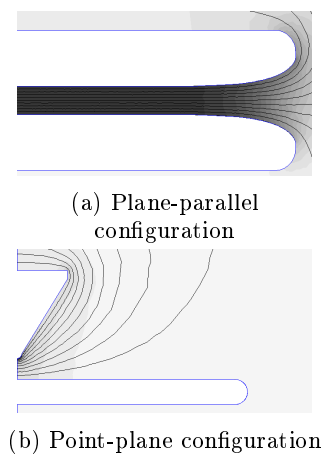


FIG. 10: Test electrodes

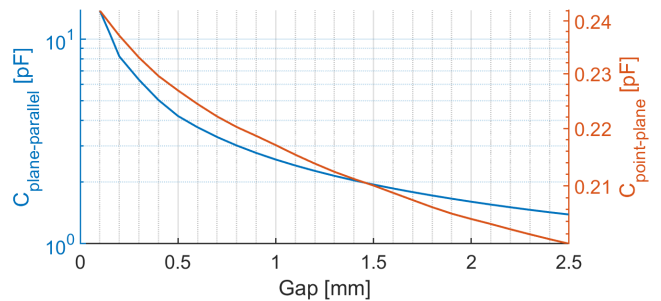


FIG. 11: Electrodes capacitance for the two configurations considered

Due to the small surface area, Q factor degradation can be neglected for the point-plane configuration. On the other hand, the plane-parallel electrodes introduce a large capacitance for the whole range of spacing considered. To avoid a significant decrease of performances, particular care will need to be taken for minimization of the RF resistance to ground in the case of microparticle deposition experiments.

## VII. DIAGNOSTIC FOR FIELD EMISSION CURRENT

### A. Field emission current in RF regime

For sufficiently high surface electric field, electrons can tunnel through the potential barrier and give rise to a field emitted current. In high voltage vacuum systems, this current controls fundamental parameters of arc formation such as field emitter evaporation and Coulomb explosion, thus playing a major role as precursor to the breakdown<sup>21</sup>. The Fowler-Nordheim expression provides the field emission current density for a given work function ( $\phi$ ), macroscopic electric field ( $E$ ) and enhancement factor ( $\beta$ ). The simplified expression given by Wang and Loew<sup>22</sup> reads:

$$j_{FE} = \frac{1.54 \cdot 10^{-6} \cdot 10^{4.52\phi^{-0.5}} (\beta E)^2}{\phi \exp\left(\frac{-6.53 \cdot 10^9 \phi^{1.5}}{\beta E}\right)}. \quad (7)$$

Since the tunnelling time is extremely short with respect to the RF period, it can be assumed that the field emission process is the same as in the DC regime. Thus, if a time-varying electric field is applied to a plane-parallel electrode configuration, current will be field emitted alternately from the two electrodes for the negative half period, responding to the instantaneous electric field. If contaminants are introduced, there is a probability that they will turn into field emitters, thus increasing  $\beta$  - and emitting area - for a specific electrode.

## B. Current-measurement circuit

To measure the field emission current in the nA range, a device consisting of a low-pass filter followed by a high gain transimpedance amplifier was developed. The voltage output - proportional to the average field emission current over one RF period - is then monitored through a low noise multimeter with large dynamic range. The current-measurement circuit is connected to the resonator through the bias-tee (figure 1-D), which provides RF insulation. The additional low-pass filter is used prior to the transimpedance amplifier to reduce the RF input signal below the noise floor level. Given the extreme sensitivity of field emission on the local electric field, a variation of 1% between the two  $\beta$  already leads to a negligible current emitted from the electrode with the lower value (figure 12). In principle it will thus be possible to discriminate the field emitting electrode with this setup.

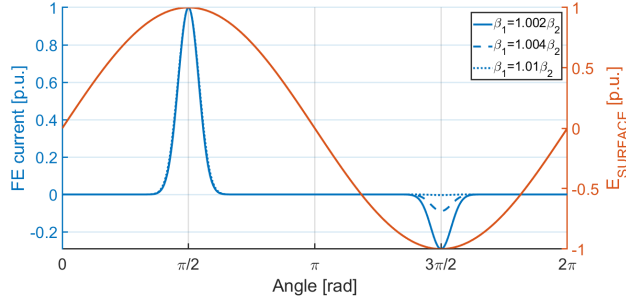


FIG. 12: Field emission current during one RF period on plane-parallel configuration, with different  $\beta$  on the two electrodes

## VIII. PRELIMINARY TESTS ON IBEX

### A. Measurement of Q factor

Quality factor measurements were carried out on IBEX to compare the simulated results with the actual setup performances. The loaded Q was computed from the  $S_{11}$  parameter, measured with a network analyzer. Central frequency is determined from the minimum of  $S_{11}$  amplitude, whereas the -3dB points are found as maximum and minimum of  $S_{11}$  imaginary part, after correction of the phase offset in the Smith chart. The maximum Q factor, i.e. measured without the loading effect introduced by the electrodes capacitance, is 830. This value is 83% of the simulated Q, leading to a reduction of 10% on the maximum achievable voltage at the open end with respect to the value obtained from circuit analysis.

### B. RF resistance to ground

The Q factor of the resonator was measured for varying  $C_{EL}$ , to investigate the effect of its degradation in relation with the magnitude of RF resistance to ground. To observe the effect over a large range of capacitances, two electrodes sets have been used:

- plane-parallel electrodes:  $C_{EL} \gtrsim 1\text{pF}$
- plane-sphere electrodes:  $C_{EL} \lesssim 1\text{pF}$

Figure 13 shows the measured Q factor, in comparison with the results obtained from simulations. Referring to the capacitance of the test electrodes considered (figure 11), it is clear that for the plane-parallel configuration the RF resistance to ground will need to be reduced, to avoid excessive degradation of Q.

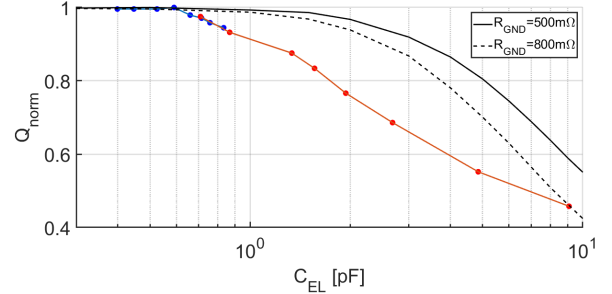


FIG. 13: Measured Q factor with varying electrodes capacitance, and comparison with simulated values

### C. Multipactor

Multipactor can be used as a conditioning tool to remove adsorbed contaminants from the electrodes. The currents generated from ionization of the desorbed gases, which affect the field emission measurements, can then be suppressed.

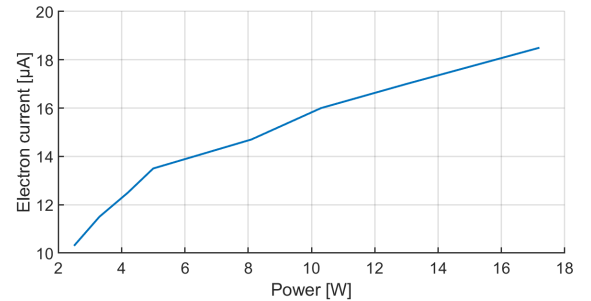


FIG. 14: Multipactor current measured with an electron probe biased at 100 V, positioned at the open-end of the resonator

Multipactor has been characterized for IBEX at resonant conditions and  $50\ \Omega$  matching at low input power, by monitoring the forward and reflected power, pressure, electron current collected from a positively biased probe and total current flowing through the bias-tee DC circuit. Electron resonance is observed for an input range of  $2.5\div 17\ \text{W}$ . After the onset of the multipactor, the input power is almost entirely reflected, accompanied by an increase in pressure. A current increasing with the power applied is observed both at the electron probe (figure 14) and through the DC circuit of the bias-tee. At higher power levels, in the  $300\div 500\ \text{W}$  range, a small current flowing in the opposite direction with respect to the multipactor case is measured at the bias-tee, without increase in reflected power; a pressure surge is observed, but of smaller magnitude compared to the multipactor conditions. This phenomenon is probably correlated to desorption and subsequent ionization of the gases<sup>23</sup>.

## IX. CONCLUSION

We have designed and built a device for the fundamental study of RF vacuum breakdown, in application to ICRF antennas. The facility is able to produce a peak voltage of 48 kV with variable electrode gap spacing, at a frequency of 54 MHz. Experimental work will be focused on the effect of particulates commonly observed in magnetic confinement fusion devices on voltage holding, and the associated field emission current.

## X. DATA AVAILABILITY

The data that support the findings of this study are available from the corresponding author upon reasonable request.

- <sup>1</sup>J.-M. Noterdaeme, A. Messiaen, R. Ragona, W. Zhang, A. Bader, F. Durodié, U. Fischer, T. Franke, E. Smigelskis, J. Ongena, M. Tran, D. Van Eester, and M. Van Schoor, "Progress on an ion cyclotron range of frequency system for demo," *Fusion Engineering and Design* **146**, 1321 – 1324 (2019), sI:SOF7-30.
- <sup>2</sup>F. Durodié, M. Vrancken, R. Bamber, L. Colas, P. Dumortier, D. Hancock, S. Huygen, D. Lockley, F. Louche, R. Maggiora, D. Milanesio, A. Messiaen, M. P. S. Nightingale, M. Shannon, P. Tigwell, M. Van Schoor, D. Wilson, K. Winkler, and C. Team, "Performance assessment of the iter icrf antenna," *AIP Conference Proceedings* **1580**, 362–365 (2014), <https://aip.scitation.org/doi/pdf/10.1063/1.4864563>.
- <sup>3</sup>G. Federici, "Plasma wall interactions in ITER," *Physica Scripta* **T124**, 1–8 (2006).
- <sup>4</sup>V. Bobkov, J.-M. Noterdaeme, F. Wesner, R. Wilhelm, and ASDEX Upgrade Team, "Influence of the plasma on icrf antenna voltage limits," *Journal of Nuclear Materials* **313-316**, 956 – 961 (2003), *plasma-Surface Interactions in Controlled Fusion Devices* 15.

- <sup>5</sup>R. Latham, *High Voltage Vacuum Insulation: Basic Concepts and Technological Practice* (Elsevier Science, 1995).
- <sup>6</sup>V. Rohde, M. Balden, T. Lunt, and the ASDEX Upgrade Team, "Dust investigations at ASDEX upgrade," *Physica Scripta* **T138**, 014024 (2009).
- <sup>7</sup>M. Balden, N. Endstrasser, P. Humrickhouse, V. Rohde, M. Rasinski, U. von Toussaint, S. Elgeti, and R. N. and, "Collection strategy, inner morphology, and size distribution of dust particles in ASDEX upgrade," *Nuclear Fusion* **54**, 073010 (2014).
- <sup>8</sup>A. Autricque, *Dust transport in tokamaks*, Ph.D. thesis, Aix-Marseille (2018).
- <sup>9</sup>R. Smirnov, S. Krashennnikov, A. Pigarov, D. Benson, M. Rosenberg, and D. Mendis, "Modeling of velocity distributions of dust in tokamak edge plasmas and dust-wall collisions," *Journal of Nuclear Materials* **390-391**, 84 – 87 (2009), proceedings of the 18th International Conference on Plasma-Surface Interactions in Controlled Fusion Device.
- <sup>10</sup>F. Höhn, W. Jacob, R. Beckmann, and R. Wilhelm, "The transition of a multipactor to a low-pressure gas discharge," *Physics of Plasmas* **4**, 940–944 (1997), <https://doi.org/10.1063/1.872564>.
- <sup>11</sup>M. Margraf, "Qucsstudio - a free and powerful circuit simulator,"
- <sup>12</sup>F. Brochard, V. Rohde, T. Lunt, G. Suárez López, A. Shalpegin, and R. Neu, "Intrinsic dust transport in asdex upgrade studied by fast imaging," *Nuclear Materials and Energy* **18**, 268 – 274 (2019).
- <sup>13</sup>S. Ratynskaia, C. Castaldo, K. Rypdal, G. Morfill, U. de Angelis, V. Pericoli-Ridolfini, A. Rufoloni, and E. Giovannozzi, "Hyper-velocity dust impacts in ftu scrape-off layer," *Nuclear Fusion* **48**, 015006 (2008).
- <sup>14</sup>M. Tang, J. Hu, J. Li, Y.-F. Li, G. Morfill, and N. Ashikawa, "Recent researches on dust in east and ht-7 tokamaks," *Journal of nuclear materials* **415**, S1094–S1097 (2011).
- <sup>15</sup>J. C. Slattery, J. F. Friichtenicht, and D. O. Hansen, "High-voltage breakdown initiated by particle impact," *Applied Physics Letters* **7**, 23–25 (1965), <https://doi.org/10.1063/1.1754238>.
- <sup>16</sup>A. K. Chakrabarti and P. A. Chatterton, "Microparticle trigger discharges and impact damage in a high-voltage vacuum insulated gap," *Journal of Applied Physics* **47**, 5320–5328 (1976), <https://doi.org/10.1063/1.322555>.
- <sup>17</sup>M. Stübig, G. Schäfer, T.-M. Ho, R. Srama, and E. GrünGrün, "Laboratory simulation improvements for hypervelocity micrometeorite impacts with a new dust particle source," *Planetary and Space Science* **49**, 853 – 858 (2001), *asteroids, Meteorites, Impacts and their Consequences (AMICO 2000)*.
- <sup>18</sup>H. Shelton, C. Hendricks Jr, and R. Wuerker, "Electrostatic acceleration of microparticles to hypervelocities," *Journal of Applied Physics* **31**, 1243–1246 (1960).
- <sup>19</sup>T. Trottenberg, H. Kersten, and H. Neumann, "Feasibility of electrostatic microparticle propulsion," *New Journal of Physics* **10**, 063012 (2008).
- <sup>20</sup>R. L. Kustom, "Effect of radio-frequency fields on the electrical breakdown of vacuum-insulated electrodes," *Journal of Applied Physics* **41**, 3256–3268 (1970).
- <sup>21</sup>H. Timko, K. Ness Sjobak, L. Mether, S. Calatroni, F. Djurabekova, K. Matyash, K. Nordlund, R. Schneider, and W. Wuensch, "From field emission to vacuum arc ignition: A new tool for simulating copper vacuum arcs," *Contributions to Plasma Physics* **55**, 299–314 (2015).
- <sup>22</sup>J. Wang and G. Loew, "Field emission and rf breakdown in high-gradient room temperature linac structures," *Tech. Rep.* (Stanford Univ., Stanford Linear Accelerator Center, CA (US), 1997).
- <sup>23</sup>J. Tan, H. Safa, B. Bonin, and J.-M. Tessier, "Radiofrequency field-emission studies. i: Design of a microwave cavity," *Journal of Physics D: Applied Physics* **27**, 2644 (1994).